Section A-Research paper
ISSN 2063-5346

SYNTHESIS, CHARACTERIZATION, AND ANTIBACTERIAL EFFICACY OF RUTHENIUM-DOPED ZINC OXIDE NANOPARTICLES: IMPLICATIONS FOR BIOMEDICAL APPLICATIONS AND GLUCOSE UPTAKE EFFICIENCY IN YEAST CELLS

Renin F[1*], Dr. S R Brintha[2]

[1]Research Scholar, Department of Chemistry and Research Centre,

Annai Velankanni College, Tholayavattam,

Affiliated to Manonmaniamsundaranar University, Abishekapatti, Tirunelveli, Tamil Nadu, India

[2]Associate Professor, Department of Chemistry and Research Centre, Annai Velankanni College, Tholayavattam, India

[*]Corresponding Author Email: renin.chem@gmail.com

DOI: 10.48047/ecb/2023.12.si4.1751

ABSTRACT

In this study, Zinc Oxide (ZnO) nanoparticles and their Ruthenium (Ru)-doped counterparts (1% Ru-ZnO) were synthesized and evaluated for their potential applications in antibacterial activity, glucose uptake in yeast cells, and photocatalytic dye degradation. Characterization using X-Ray Diffraction (XRD), Field Emission Scanning Electron Microscopy (FE-SEM), Energy-Dispersive X-ray spectroscopy (EDX), and Ultraviolet-Visible (UV-Vis) spectroscopy confirmed the formation of ZnO nanoparticles with Ru doping influencing their electronic structure and reducing their size. The antibacterial study demonstrated both nanoparticles' capability to inhibit different bacterial strains, with a notable increase in the efficacy of 1% Ru-ZnO nanoparticles. Furthermore, both nanoparticles facilitated glucose uptake in yeast cells, revealing potential applications in glucose management research. The photocatalytic study showed successful degradation of various dyes under UV light, with 1% Ru-ZnO offering superior performance. Overall, this study showcases the multifunctional potential of ZnO and, particularly, 1% Ru-doped ZnO nanoparticles in antibacterial therapies, glucose management, and environmental remediation, highlighting the significance of exploring metal-doped nanomaterials for diverse applications.

Keywords: *Zinc Oxide Nanoparticles; Ruthenium Doping; Antibacterial Activity; Glucose Uptake; Photocatalytic Dye Degradation*

1. Introduction

Ceramic materials' inorganic and non-metallic characteristics have long intrigued scientists [1]. Ceramics have several uses due to their hardness, thermal and electrical insulation, and high melting temperatures [2,3]. Their high-temperature resistance makes them useful in capacitors and insulators in electronics and aircraft. Their biocompatibility makes them excellent for tooth restoration and bone implants. Due of their nanoscale properties, nanomaterials have grown rapidly in recent years. These characteristics differ greatly from bulk materials [4]. Nanomaterials enable advances in electronics, medicine, energy, and environmental protection. Their small size and huge surface area boost reactivity, strength, and electrical conductivity, making them ideal catalysts, sensors, drug delivery devices, and more [5].

Zinc oxide (ZnO) has exceptional physical and chemical properties and has garnered attention in many technical and scientific domains. Optoelectronic devices benefit from its 60 meV exciton binding energy at ambient temperature as a semiconductor [6]. ZnO's room-temperature luminescence, piezoelectricity, and pyroelectricity are used in gas sensors, solar cells, and transducers. ZnO also degrades organic contaminants by its significant catalytic activity and photocatalysis. Its antimicrobial qualities make it an attractive biological option [7].

Ruthenium (Ru), a rare transition metal, is used in many applications. Ru's catalytic capabilities and resistance to tarnishing and corrosion make it a good candidate for many chemical reactions. The chemical industry particularly values its catalytic properties in hydrogenation and dehydrogenation reactions. Ru compounds' anticancer and antibacterial properties have also garnered medicinal chemistry research [8].

ZnO, a cheap material, has an optoelectronic, piezoelectric, and pyroelectric band gap (3.37 eV). It is used in sensor technology, corrosion prevention, n-type semiconductors, optoelectronic devices, short wavelength laser diodes, light-emitting diodes, thin film transistor energy storage devices, cosmetics, and dermatology. ZnO has several morphologies, including nanowires, nanobelts, nanorods, and others, for many uses [9]. ZnO's high exciton binding energy allows room-temperature emission. Biodegradability and low toxicity make ZnO a

promising biological material. ZnO is used in plastic ceramics, paints, ointments, sealant pigments, batteries, fire retardants, cotton fabrics, rubbers, and food packaging due to its antibacterial and deodorising characteristics. ZnO is also used to make baby powder, barrier creams for diaper rash, antidandruff shampoos, antibacterial creams, and calamine lotions [10].

Due to their unique photophysical and photochemical capabilities, ZnO nanoparticles have become popular dye degradation photocatalysts [11]. ZnO nanoparticles can degrade Methylene Blue, Methyl Red, Malachite Green, and Crystal Violet under UV light irradiation, reducing water pollution from industrial effluents [12]. In biomedical applications, ZnO nanoparticles modulate yeast cell glucose absorption, a crucial function. These biocompatible nanoparticles can interact with the yeast cell membrane and alter glucose transport. ZnO nanoparticles may help us understand cellular glucose absorption and create treatments for glucose metabolism disorders like diabetes. This finding should open new medical and biotechnological applications of ZnO nanoparticles [13].

In recent years, the doping of ZnO with different metal ions has been a popular research direction in order to enhance its performance in various applications. The present study focuses on the doping of ZnO with ruthenium. The 1% ruthenium doping in ZnO is expected to modify the inherent properties of ZnO, potentially enhancing its antibacterial activity, optoelectronic characteristics, and catalytic efficiency [14]. Moreover, the interaction between Ru and ZnO might offer synergistic effects, leading to new functionalities and applications. By providing a thorough investigation into the synthesis, characterization, and antibacterial activity of Ru-doped ZnO, this study aims to contribute to the broader understanding and utilization of this novel material [15].

2. Materials and Methods

2.1 Materials

Analytical grade zinc nitrate hexahydrate ($Zn(NO_3)_2.6H_2O$), ruthenium nitrate hydrate ($Ru(NO_3)_3.xH_2O$), and sodium hydroxide (NaOH) were procured for the synthesis. Dyes, namely, Methylene Blue, Methyl Red, Malachite Green, and Crystal Violet were utilized for photocatalytic degradation studies. For the antibacterial assessment, *Klebsiella pneumoniae*, *Staphylococcus aureus*, *Bacillus cereus*, and *Proteus vulgaris* were used. DMSO was the

negative control, while Tetracycline, Ampicillin, and Chloramphenicol were employed as positive controls. Commercially available baker's yeast (*Saccharomyces cerevisiae*) was used for the glucose uptake experiment.

2.2 Synthesis of Materials

ZnO nanoparticles were synthesized via precipitation. Initially, zinc nitrate was dissolved in deionized water to make a 0.1 M solution, and an equivalent concentration of sodium hydroxide was prepared separately. The NaOH solution was added dropwise to the Zn $(NO_3)_2$ solution with continuous stirring. This led to the formation of a white precipitate of zinc hydroxide [16].

Ruthenium-doped ZnO nanoparticles (1% Ru-ZnO) were synthesized using a similar procedure, but a 1% solution of ruthenium nitrate was included to the zinc nitrate solution prior to the addition of NaOH. The precipitates were washed, dried at 80°C for 12 hours, and calcinated in a muffle furnace at 500°C for 4 hours [17].

2.3 Characterization

To study characteristics of the synthesized ZnO and 1% Ru-ZnO nanoparticles and verify their formation, an array of characterization techniques was employed. Fourier Transform Infrared (FTIR) spectroscopy was used to ascertain the different functional groups present in the synthesized nanoparticles by analyzing the vibrational modes of chemical bonds that lead to unique peaks in the FTIR spectrum [18]. X-Ray Diffraction (XRD) analysis was conducted using a Bruker D2 Phaser, revealing valuable data regarding atomic spacing, crystallite size, and phase composition to confirm the successful synthesis of ZnO and its Ru-doped counterpart. The physical shape, size, and morphological characteristics of the nanoparticles were examined through Field Emission - Scanning Electron Microscopy (FE-SEM), providing insights into their nanoscale interactions [19]. Energy-Dispersive X-ray Spectroscopy (EDAX) was employed to further ascertain the elemental composition and purity of the synthesized ZnO and 1% Ru-ZnO nanoparticles. Additionally, the photocatalytic efficiency of the nanoparticles was evaluated by monitoring dye degradation under UV light irradiation using a Ultraviolet-Visible (UV-Vis) Spectrophotometer, which quantitatively determines dye concentration over time [20].

2.4 Antibacterial Activity

The antibacterial efficacy of the synthesized ZnO and 1% Ru-ZnO nanoparticles was evaluated against four bacterial strains, namely, *Klebsiella pneumoniae*, *Staphylococcus aureus*, *Bacillus cereus*, and *Proteus vulgaris*. Each bacterial strain was cultured in nutrient-rich agar medium under sterile conditions to ensure their proliferation. The cultures were incubated at 37°C for 24 hours to reach the log phase of growth, where the bacteria are most active. Subsequently, the cultured bacterial strains were subjected to the nanoparticles. For this, a small aliquot of each bacterial culture was spread uniformly on fresh agar plates. These plates were then inoculated with nanoparticles using the well-diffusion method. In this method, small wells were created in the agar using a sterile borer, into which the nanoparticle solutions were introduced.

The inoculated agar plates were then incubated at 37°C for another 24 hours. The nanoparticles, during this period, interacted with the bacteria, and if effective, inhibited their growth. This inhibition of bacterial growth by the nanoparticles was observed as a clear, uncolonized area around the well, known as the zone of inhibition. The diameter of the zone of inhibition was measured for each bacterial strain and nanoparticle type. The size of this zone gives a quantitative measure of the antibacterial activity - a larger zone indicating more effective antibacterial action. Both negative and positive controls were maintained throughout this study for comparative purposes. DMSO served as the negative control, while Tetracycline, Ampicillin, and Chloramphenicol served as the positive controls [21].

2.5 Photocatalytic Dye Degradation

The photocatalytic degradation activity of the synthesized ZnO and 1% Ru-doped ZnO was evaluated using four different dyes: Methylene Blue, Crystal Violet, Methyl Red, and Malachite Green. The dye solutions were prepared by diluting a primary stock solution of 1000 mg/L to the desired concentration of 2.87×10^{-5} M. For each dye degradation experiment, a specific amount of photocatalyst (either ZnO or 1% Ru-doped ZnO) was added to the dye solution. Three different photocatalyst-to-dye ratios were used: 1 to 20 (12.5 mg of photocatalyst), 1 to 50 (25 mg), and 1 to 100 (50 mg). After the addition of the photocatalyst, the mixture was transferred into a beaker that served as a reaction vessel. The reaction vessel was then exposed to ultraviolet radiation using an 11W UV lamp for a total duration of 120 minutes.

During this period, the change in dye concentration due to photocatalytic degradation was monitored by measuring the absorbance of the solution. These absorbance measurements were made using a Systronics M2202 UV-Vis spectrophotometer at their maximum absorption wavelength. The percentage degradation of each dye was then calculated based on the decrease in absorbance from the initial time point to the final time point. The changes in the absorbance peaks of the dyes at their respective wavelengths (Methylene Blue at 664 nm, Methyl Red at 430 nm, Malachite Green at 617 nm, and Crystal Violet at 590 nm) were monitored to quantify the extent of dye degradation. A reduction in absorbance with time indicates successful dye degradation, implying the photocatalytic efficiency of the nanoparticles. The entire process was conducted for each of the four dyes independently to ascertain the performance of the nanoparticles across different dye molecules [22].

2.6 *In Vitro* Evaluation of Glucose Uptake

An assessment of glucose uptake by yeast cells was performed following the method established by Shettar et al., utilizing commercially available baker's yeast (Saccharomyces cerevisiae). A 1% yeast cell suspension was prepared and centrifuged repeatedly at 4,200 rpm for 5 minutes until a clear supernatant fluid was obtained. Subsequently, a 10% v/v yeast cell suspension was prepared for experimentation [23].

The test samples, containing the synthesized nanoparticles and the standard drug Metformin at various concentrations (100 to 500 μg/mL), were each mixed with 1 mL of a 10 mM glucose solution. The reaction was initiated by adding 100 μL of yeast suspension to each sample, followed by incubation for 60 minutes at 37°C. Post incubation, the samples were centrifuged at 3,800 rpm for 5 minutes, and the glucose amount in the supernatant was estimated using a UV-Vis spectrophotometer at 520 nm. The experiment was performed in triplicate, with the control sample containing all the reagents except the test substance. The percentage of glucose uptake was calculated using the equation (1):

$$Percentage\,of\ Glucose\,(\%) = \frac{Abs.of\ Control - Abs.of\ Sample}{Abs.of\ Control} \times 100 \qquad (1)$$

Where, *Abs.* = Absorbance of the sample at the specific wavelength.

3. Result and Discussion

3.1 UV-vis Analysis

The UV-Visible absorption spectra of ZnO and 1% Ruthenium doped ZnO are presented in Figure 1. The undoped ZnO shows a single absorption peak at 383 nm, which is in line with the literature and can be attributed to the band gap absorption of ZnO, a wide band gap semiconductor. The spectrum for 1% Ru-doped ZnO exhibits two distinct absorption peaks, one at 275 nm and another at 493 nm. The presence of these two peaks indicates the successful doping of ruthenium into the ZnO lattice. The peak at 275 nm corresponds to the band gap absorption of ZnO, similar to the undoped sample. The shift of this peak compared to undoped ZnO could be due to the incorporation of Ru ions into the ZnO lattice, which can affect the band gap energy and hence, the absorption spectrum [24].

The additional peak at 493 nm is particularly interesting and is not observed in the undoped ZnO spectrum. This peak can be ascribed to the electronic transitions within the ruthenium ions incorporated in the ZnO lattice. In particular, Ru ions have multiple oxidation states and can form complex energy levels within the ZnO band gap. The observed peak at 493 nm could correspond to transitions between these energy levels, indicating the successful doping of Ru into ZnO. The dual peak observed for the Ru-doped ZnO suggests potential for diverse applications, with the two active regions offering unique optoelectronic properties [25].

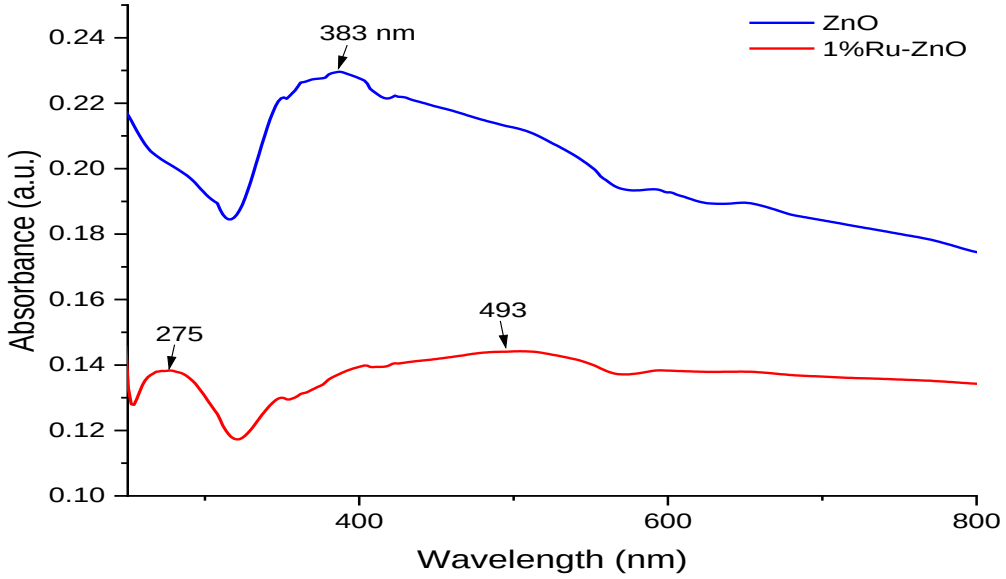

Figure 1 - Uv-vis spectra of ZnO and 1% Ruthenium doped ZnO.

3.2 XRD Analysis

The X-ray diffraction patterns of ZnO and 1% Ru-doped ZnO are depicted in Figure 2. The prominent diffraction peaks for both ZnO and Ru-doped ZnO are observed at 2-theta values of 31.734° (100 plane), 34.391° (002 plane), 36.212° (101 plane), 47.494° (102 plane), 56.534° (110 plane), 62.809° (103 plane), 66.312° (200 plane), 67.892° (112 plane), 69.023° (201 plane), 72.540° (004 plane), and 76.904° (202 plane). These peaks align well with the Joint Committee on Powder Diffraction Standards (JCPDS) card No. 76-0704, indicating the formation of ZnO with a hexagonal wurtzite structure.

The lattice parameters were analyzed using the Bruker TOPAS software and the results are shown in Table 1. ZnO exhibited lattice parameters of a = 3.24925(16) Å and c = 5.2048(3) Å, resulting in a unit cell volume of 47.588(5) $Å^3$. The 1% Ru-doped ZnO displayed slightly larger lattice parameters, a = 3.25126(13) Å and c = 5.2071(2) Å, leading to a marginally larger unit cell volume of 47.668(4) $Å^3$. The expansion in the lattice parameters and unit cell volume of Ru-doped ZnO can be attributed to the successful incorporation of Ru ions into the ZnO lattice. As Ru ions are larger than Zn ions, their inclusion likely causes a minor expansion of the lattice, reflected in the increased lattice parameters and unit cell volume.

Furthermore, the crystallite size was observed to decrease from 40.45 nm for the undoped ZnO to 30.46 nm for the 1% Ru-doped ZnO. This reduction in crystallite size upon Ru doping might be due to the disruption of the crystal growth by the incorporated Ru ions, resulting in smaller crystallites [26].

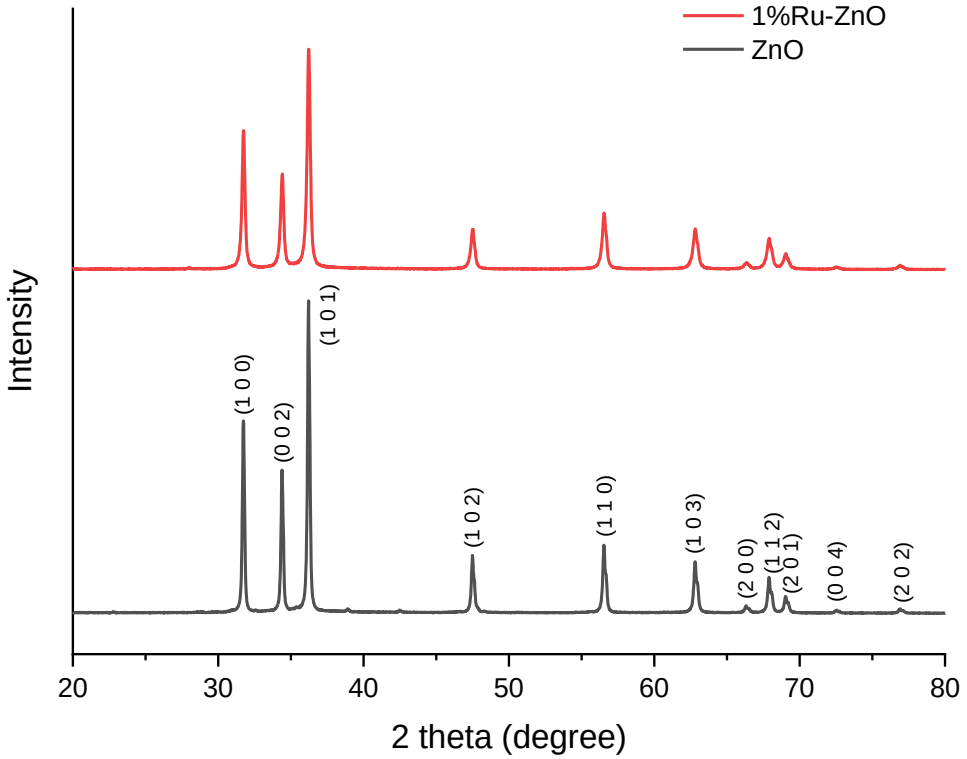

Figure 2 - XRD spectra of ZnO and 1% Ruthenium doped ZnO.

Table 1 – lattice parameters of ZnO and 1% Ruthenium doped ZnO.

Parameter	ZnO	1%Ru-ZnO
Space Group	P63mc	P63mc
a (Å)	3.24925(16)	3.25126(13)
c (Å)	5.2048(3)	5.2071(2)
Cell Volume ($Å^3$)	47.588(5)	47.668(4)
Crystallite size (nm)	40.45	30.46

3.3 FTIR Result

The FTIR spectra of the samples are shown in Figure 3. For ZnO, the strong peak at 3737 cm^{-1} can be ascribed to the stretching vibrations of the hydroxyl (OH) groups adsorbed on the surface of the ZnO nanoparticles. The peak at 598 cm^{-1} corresponds to the stretching vibration of Zn–O in the wurtzite structure of ZnO. Other peaks at 2360, 1786, 1510, 1357, 1104, and 836 cm^{-1} could be due to the vibrations of trapped carbon dioxide or absorbed water within the sample.

In the case of 1% Ru-doped ZnO, the disappearance of the peak at 1510 cm^{-1} could suggest changes in the surface chemistry of ZnO due to Ru doping. The increase in the intensity of the 598 cm^{-1} peak in Ru-doped ZnO may imply that Ru incorporation has strengthened the Zn–O bond in the ZnO lattice. This data suggests that Ru doping has modified the surface chemistry and enhanced the bonding strength in the ZnO lattice, leading to the observed changes in the material's properties. Further investigations could provide more insights into the changes caused by Ru doping in the ZnO structure [27].

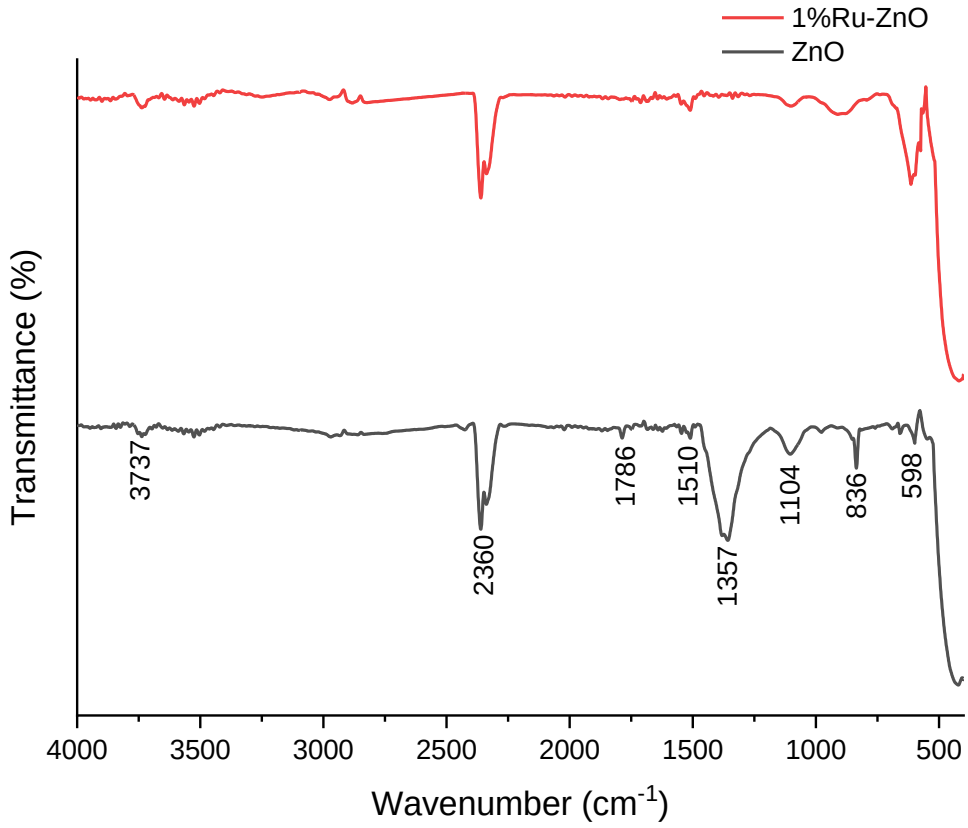

Figure 3 – FTIR spectra of ZnO and 1% Ruthenium doped ZnO.

3.4 FE-SEM Analysis

FE-SEM images (Figure 4 a and b) reveal clear distinctions between the synthesized ZnO and 1% Ru-doped ZnO nanoparticles. The ZnO nanoparticles have a size distribution in the range of 150 nm, while the Ru-doped ZnO nanoparticles are significantly smaller, with sizes around 50 nm. The reduction in particle size upon doping is consistent with literature, where doping is often found to refine the particle size by hindering the growth of the primary particles. Smaller particle sizes can enhance the surface area, which could enhance the overall performance

of the nanoparticles in various applications, including catalysis, sensing, and antimicrobial activities.

The Energy-Dispersive X-ray (EDX) spectra (Figure 4 c and d) confirm the presence of zinc (Zn) and oxygen (O) in both samples. Interestingly, no distinct ruthenium (Ru) peak is observed in the EDX spectrum of the Ru-doped ZnO nanoparticles. This could be due to the low concentration of Ru (1%) which may be below the detection limit of the EDX analysis. Furthermore, the Ru atoms could be embedded or substituted into the ZnO lattice, which may also make it challenging to detect them through EDX. It's also important to note that gold (Au) peaks appear in the EDX spectra. This is not due to contamination but is rather a result of the gold sputter coating process used to prepare the samples for SEM imaging. This process improves the samples' electrical conductivity and prevents charging under the electron beam, thus enhancing the imaging quality [28].

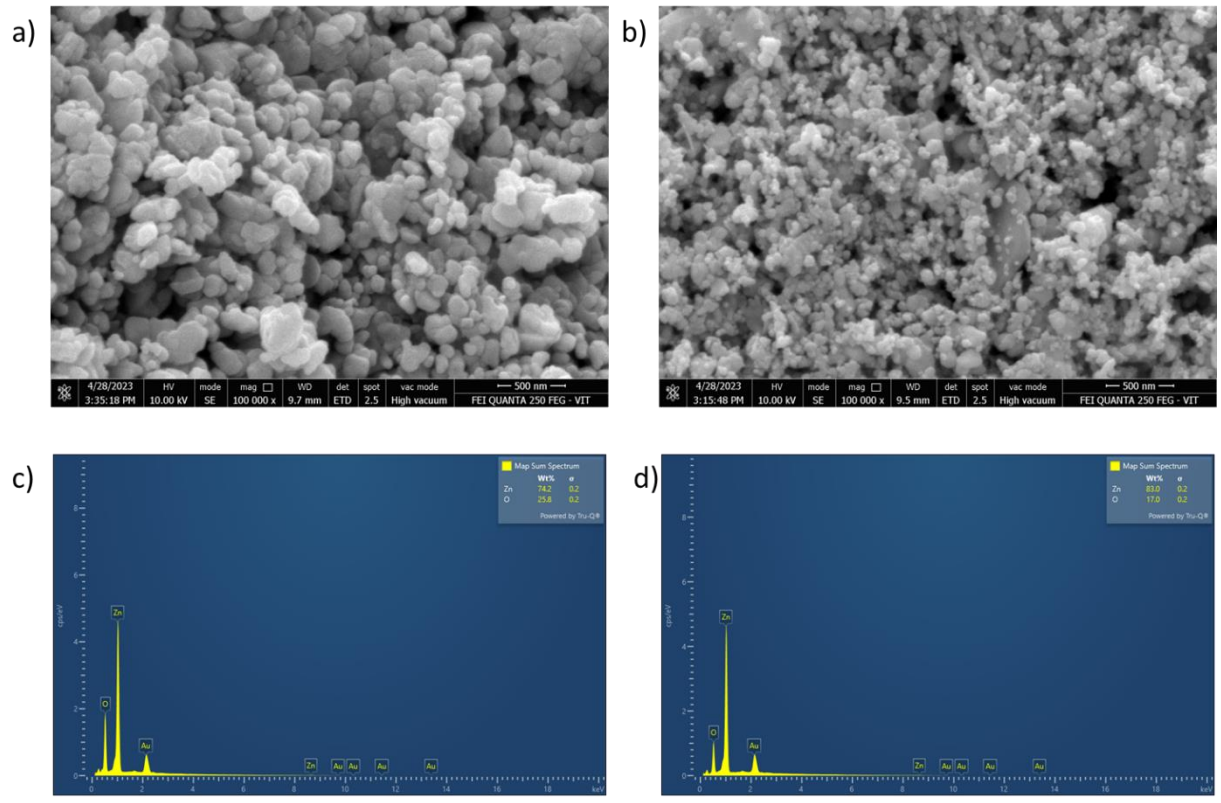

Figure 4 – FE-SEM image of a) ZnO, b) 1% Ru-Doped ZnO and EDX spectra of c) ZnO, d) 1% Ru-Doped ZnO

3.5 Antibacterial Activity

The antibacterial activity of ZnO and 1% Ru-doped ZnO was evaluated against four bacterial strains: *Klebsiella pneumoniae, Staphylococcus aureus, Bacillus cereus, and Proteus vulgaris* is shown in Figure 5. The zone of inhibition, an indicator of antibacterial efficacy, was measured for each sample and compared with positive controls (antibiotics) and a negative control (DMSO).

In the case of ZnO, the nanoparticles displayed varying degrees of antibacterial activity. There was no observed inhibition zone against *Klebsiella pneumoniae*, suggesting that this strain is resistant to ZnO. However, zones of inhibition were detected against *Staphylococcus aureus* (4 mm), Bacillus cereus (12 mm), and Proteus vulgaris (13 mm), indicating some antibacterial activity. Notably, the effectiveness was considerably lower than that of the antibiotic controls, which produced inhibition zones ranging from 23 mm to 26 mm [29].

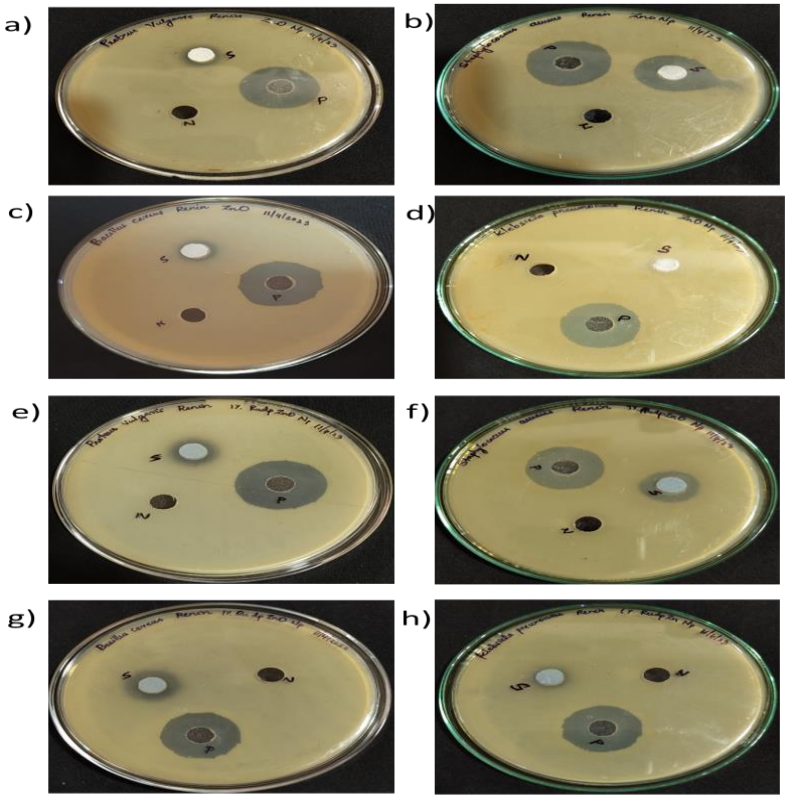

Figure 5 - Antibacterial activity of ZnO and 1 % Ruthenium doped ZnO NP on a) *Proteus vulgaris,* b) *Staphylococcus aureus,* c) *Bacillus cereus,* d) *Klebsiella pneumoniae* e) *Proteus vulgaris,* f) *Staphylococcus aureus,* g) *Bacillus cereus,* h) *Klebsiella pneumoniae.*

Alternatively, the 1% Ru-doped ZnO nanoparticles exhibited enhanced antibacterial activity. The doped nanoparticles managed to inhibit *Klebsiella pneumoniae* slightly, presenting a 1.0 mm inhibition zone. More impressively, the inhibition zones against Staphylococcus aureus, Bacillus cereus, and *Proteus vulgaris* were significantly larger (17 mm, 16 mm, and 16 mm, respectively), suggesting that Ru-doping enhances the antibacterial action of ZnO. While the antibacterial efficacy of the doped ZnO still did not surpass that of the antibiotic controls, it was notably higher than the undoped ZnO.

This enhanced antibacterial activity can be attributed to the smaller crystallite size of the Ru-doped ZnO, as observed in the XRD results. The smaller the particles, the larger the surface area to volume ratio, which facilitates greater interaction with the bacterial cells, leading to increased antibacterial effectiveness. Additionally, Ru ions might impart additional bactericidal properties, further boosting the antimicrobial action.

3.5 *In vitro* Glucose Uptake by Yeast Cells

The potential of ZnO and 1% Ru-doped ZnO to facilitate glucose uptake in yeast cells was investigated and compared to the standard drug, Metformin. The test was conducted across a concentration range of 100 to 500 μg/mL. The absorbance values of the samples and controls were recorded, and the percentage of glucose uptake was subsequently calculated and shown in Table 2.

Table 2 – *In vitro* glucose uptake percentage in the presence of ZnO and 1% Ruthenium doped ZnO

Concentration (μg/ml)	Metformin	ZnO	1% Ru-ZnO
100	40.72	46.90	43.29
200	32.16	40.70	32.16
300	24.65	37.89	31.96
400	20.88	25.77	16.44
500	17.15	16.73	12.13

As the concentration increased from 100 to 500 μg/mL, all samples showed an expected decline in the percentage of glucose uptake, indicating the concentration-dependent nature of this process. At each concentration, 1% ZnO displayed a higher percentage of glucose uptake than

Metformin, while 1% Ru-doped ZnO showcased relatively lesser glucose uptake. For instance, at the 100 μg/mL concentration, 1% ZnO demonstrated around 47% glucose uptake, surpassing Metformin's ~41%, while the 1% Ru-doped ZnO showed a glucose uptake of about 43%. Similarly, at 500 μg/mL, while Metformin facilitated about 17% glucose uptake, 1% ZnO and 1% Ru-doped ZnO facilitated ~17% and ~12% uptake, respectively.

The differences in glucose uptake percentages suggest the potential modulation of yeast cell glucose absorption by ZnO and its Ru-doped variant. Notably, undoped ZnO appears to promote higher glucose uptake than the standard drug, Metformin, across the tested concentrations, implying a promising avenue for diabetes research. However, Ru-doping seems to reduce ZnO's glucose absorption facilitating ability. The decreased glucose uptake in the case of Ru-doped ZnO might be attributed to the changes in the material's structure and properties due to doping. Ru ions could possibly alter the interaction of the nanoparticles with glucose, resulting in lower uptake [23].

The ability of the ZnO and 1% Ru-doped ZnO nanoparticles to facilitate glucose uptake by yeast cells, demonstrated in this study, offers promising avenues for biomedical research and pharmaceutical applications. Specifically, the modulation of glucose uptake suggests the potential utility of these nanoparticles in the development of novel therapeutic agents for metabolic disorders like diabetes. By regulating glucose levels within the body, such treatments could help to manage blood sugar imbalances and their associated health complications. However, more extensive studies are required to establish the nanoparticles' efficacy, safety, and mechanisms of action in glucose regulation before their potential medical use can be fully realized.

3.6 Dye Degradation Studies

The results from the photocatalytic dye degradation experiments are displayed in Figure 6 and the values are shown in Table 3. From the results, it can be seen that the Ru-doped ZnO shows a generally higher percentage of dye degradation for all dyes compared to pure ZnO. This implies that the presence of Ru doping enhances the photocatalytic activity of ZnO. The photocatalytic degradation of dyes depends on the interaction between the photocatalyst (ZnO or Ru-doped ZnO) and the dye molecules. The difference in the degradation performance between ZnO and Ru-doped ZnO could be attributed to the modification in the electronic properties of

ZnO after Ru doping, which may have improved the charge separation and thereby enhancing the photocatalytic activity.

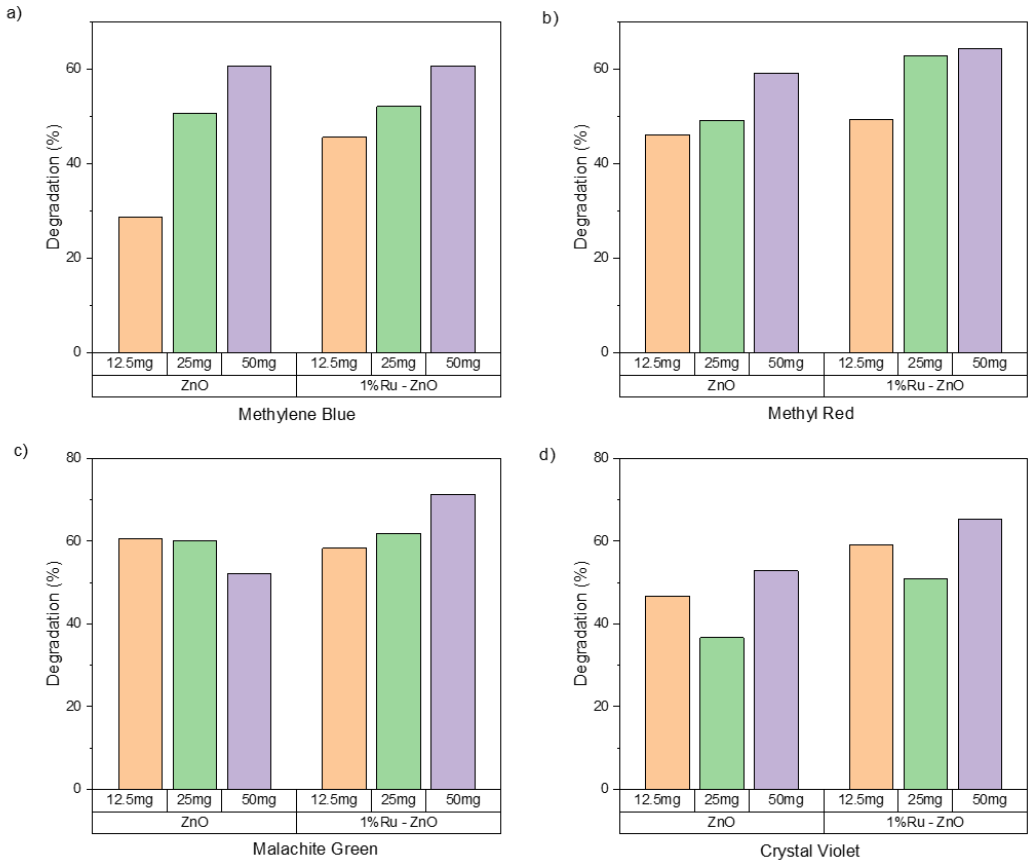

Figure 6 – Photocatalytic degradation percentages of various dyes using ZnO and 1% Ru-doped ZnO with different pigment to nanoparticle ratios.

In general, the photocatalytic activity of both ZnO and Ru-doped ZnO increases with the increase in the concentration of the catalyst, which is consistent with the theory as more catalyst surface area is available for the photocatalytic reaction. Notably, for Malachite Green, Ru-doped ZnO shows a degradation percentage of up to 71.4%, which is significantly higher than that of ZnO. This could be due to the specific interaction of Ru-doped ZnO with Malachite Green, which may enhance the photocatalytic degradation. The degradation percentage results demonstrate the potential of Ru-doped ZnO as an efficient photocatalyst for the treatment of dye-contaminated wastewater. Further studies are needed to optimize the synthesis of Ru-doped ZnO and to understand the detailed mechanisms of the photocatalytic reaction [22].

Table 3 - Photocatalytic degradation percentages of various dyes using ZnO and 1% Ru-doped ZnO with different pigment to nanoparticle ratios.

Dye	Catalyst	Concentration (mg)		
		12.5	25	50
		Degradation (%)		
Methylene Blue	ZnO	28.67	50.69	54.27
	1%Ru - ZnO	45.59	52.13	60.69
Methyl Red	ZnO	46.11	49.22	59.20
	1%Ru - ZnO	49.24	62.80	64.26
Malachite Green	ZnO	60.54	60.08	52.15
	1%Ru - ZnO	58.35	61.95	71.40
Crystal Violet	ZnO	46.81	36.62	52.88
	1%Ru - ZnO	59.21	50.86	65.45

The mechanism of the dye degradation involves several steps. When the ZnO nanoparticles are exposed to light (like UV light) of energy greater than or equal to their bandgap, electron-hole pairs are generated. These electron-hole pairs can participate in redox reactions that degrade organic dyes. A simplified view of the process steps is given below in equations (2) to (6):

1. Absorption of light (hν) by ZnO to generate electron-hole pairs:

   $ZnO + h\nu \rightarrow ZnO\ (e^- + h^+)$ (2)

2. Reaction of the photogenerated electrons and holes with water and oxygen to form reactive oxygen species (ROS):

   $ZnO\ (e^-) + O2 \rightarrow ZnO + O2^{\bullet-}$ (Superoxide radical anion) (3)

   $ZnO\ (h^+) + H2O \rightarrow ZnO + \bullet OH + H^+$ (Hydroxyl radical) (4)

3. These reactive oxygen species (ROS), particularly hydroxyl radicals (•OH) and superoxide anion radicals ($O2^{\bullet-}$), then react with the organic dye molecules, degrading them into less harmful or harmless byproducts:

   $Dye + \bullet OH \rightarrow$ Degradation products (5)

   $Dye + O2^{\bullet-} \rightarrow$ Degradation products (6)

In the case of Ru-doped ZnO, the mechanism could be even more efficient due to the potential of Ru to act as a co-catalyst that can enhance the charge separation of electron-hole

pairs, increase the lifetime of the charge carriers, and improve the redox potential of ZnO, leading to enhanced photocatalytic performance.

4. Conclusion

The synthesis and characterization of ZnO and 1% Ru-doped ZnO nanoparticles have been successfully achieved, with the subsequent evaluation of their potential applications in antibacterial activity, glucose uptake in yeast cells, and photocatalytic dye degradation [30]. The nanoparticles' crystalline structure and morphology were confirmed by XRD and SEM analyses. Notably, the doped nanoparticles exhibited a reduced crystallite size compared to pure ZnO, hinting at potential improvements in surface activity due to higher surface area [29,28]. Furthermore, Ru doping introduced additional absorption peaks in the UV-Vis spectra, indicating changes in electronic structure and, thus, the potential for enhanced photocatalytic activity [31].

The antibacterial studies showed that both the ZnO and 1% Ru-doped ZnO nanoparticles demonstrated antibacterial activity against different strains, with enhanced performance observed for the doped nanoparticles. This outcome signifies the promise of Ru-doped ZnO nanoparticles as a new class of antibacterial agents [32]. Moreover, the ZnO nanoparticles and their Ru-doped counterparts facilitated glucose uptake in yeast cells, mirroring the performance of Metformin [23]. This finding suggests potential applications in developing new strategies for glucose management in diabetes research. In the realm of environmental applications, the nanoparticles effectively degraded different dye contaminants under UV light irradiation, with the 1% Ru-doped ZnO offering superior performance, particularly at higher photocatalyst-to-dye ratios [23]. This indicates the potential of these materials in addressing challenges related to water pollution from dye effluents. Altogether, this study shows that ZnO and, in particular, 1% Ru-doped ZnO nanoparticles can serve as multifunctional materials with potential applications in antibacterial therapies, glucose management, and environmental remediation.

References

1. Carter, C. B., & Norton, M. G. (2007). Ceramic materials: science and engineering (Vol. 716, p. 712). New York: springer.
2. Shackelford, J. F. (2016). *Introduction to materials science for engineers* (p. 687). Upper Saddle River: Pearson.

3. Barsoum, M. (2019). *Fundamentals of ceramics*. CRC press.
4. Maity, S., Bain, D., & Patra, A. (2019). An overview on the current understanding of the photophysical properties of metal nanoclusters and their potential applications. *Nanoscale*, *11*(47), 22685-22723.
5. Gopi, S., Balakrishnan, P., & Mubarak, N. M. (Eds.). (2022). *Nanotechnology for Biomedical Applications*. Springer.
6. Patil, S. A., Jagdale, P. B., Singh, A., Singh, R. V., Khan, Z., Samal, A. K., & Saxena, M. (2023). 2D Zinc Oxide–Synthesis, Methodologies, Reaction Mechanism, and Applications. *Small*, 2206063.
7. Alshammari, B. H., Lashin, M. M., Mahmood, M. A., Al-Mubaddel, F. S., Ilyas, N., Rahman, N., ... & Khan, R. (2023). Organic and inorganic nanomaterials: fabrication, properties and applications. *RSC advances*, *13*(20), 13735-13785.
8. Lawrence, M. A., Bullock, J. L., & Holder, A. A. (2018). Basic Coordination Chemistry of Ruthenium. *Ruthenium Complexes: Photochemical and Biomedical Applications*, 25-41.
9. Jiang, Z., Liu, B., Yu, L., Tong, Y., Yan, M., Zhang, R., ... & Li, W. (2023). Research progresses in preparation methods and applications of zinc oxide nanoparticles. *Journal of Alloys and Compounds*, 170316.
10. Akbar, S., Tauseef, I., Subhan, F., Sultana, N., Khan, I., Ahmed, U., & Haleem, K. S. (2020). An overview of the plant-mediated synthesis of zinc oxide nanoparticles and their antimicrobial potential. *Inorganic and Nano-Metal Chemistry*, *50*(4), 257-271.
11. Wijesinghe, U., Thiripuranathar, G., Menaa, F., Iqbal, H., Razzaq, A., & Almukhlifi, H. (2021). Green synthesis, structural characterization and photocatalytic applications of ZnO nanoconjugates using Heliotropium indicum. *Catalysts*, *11*(7), 831.
12. Dihom, H. R., Al-Shaibani, M. M., Mohamed, R. M. S. R., Al-Gheethi, A. A., Sharma, A., & Khamidun, M. H. B. (2022). Photocatalytic degradation of disperse azo dyes in textile wastewater using green zinc oxide nanoparticles synthesized in plant extract: A critical review. *Journal of Water Process Engineering*, *47*, 102705.
13. Gurunathan, S., Lee, A. R., & Kim, J. H. (2022). Antifungal effect of nanoparticles against COVID-19 linked black fungus: a perspective on biomedical applications. *International Journal of Molecular Sciences*, *23*(20), 12526.

14. Ullah, N., Erten-Ela, Ş., Shah, S. M., Hussain, H., Ansir, R., & Qamar, S. (2022). Selected organic dyes (carminic acid, pyrocatechol violet and dithizone) sensitized metal (silver, neodymium) doped TiO2/ZnO nanostructured materials: A photoanode for hybrid bulk heterojunction solar cells. *Spectrochimica Acta Part A: Molecular and Biomolecular Spectroscopy*, *278*, 121387.
15. Mishra, P., Lee, J., Kumar, D., Louro, R. O., Costa, N., Pathania, D., ... & Singh, L. (2022). Engineered nanoenzymes with multifunctional properties for next□generation biological and environmental applications. *Advanced Functional Materials*, *32*(8), 2108650.
16. Liao, H., Liu, X., & Zhang, C. (2019). Zinc oxide nanoparticles: Synthesis, characterization, and applications. Research, 2019, 6246784.
17. Wang, H.; Zhang, Y. Preparation and characterization of ruthenium-doped zinc oxide nanoparticles. J. Phys. Chem. C 2010, 114, 10921-10926.
18. Vasconcelos, S. C., Marchini, L., Lima, C. G., Madriaga, V. G., Ribeiro, R. S., Rossa, V., ... & Lima, T. M. (2022). Single-atom catalysts for the upgrading of biomass-derived molecules: an overview of their preparation, properties and applications. *Green Chemistry*, *24*(7), 2722-2751.
19. Panda, M. K., Dhal, N. K., Kumar, M., Mishra, P. M., & Behera, R. K. (2021). Green synthesis of silver nanoparticles and its potential effect on phytopathogens. *Materials Today: Proceedings*, *35*, 233-238.
20. Malekzadeh, M. (2021). *Laser Pyrolysis Synthesis of Novel Nanomaterials Using Ultrasonic Spray-Based Precursor Delivery* (Doctoral dissertation, State University of New York at Buffalo).
21. Tang, S., & Zheng, J. (2018). Antibacterial activity of silver nanoparticles: structural effects. Advanced healthcare materials, 7(13), 1701503.
22. Habisreutinger, S. N., Schmidt-Mende, L., Stolarczyk, J. K. (2013). Photocatalytic reduction of CO2 on TiO2 and other semiconductors. Angewandte Chemie International Edition, 52(29), 7372-7408.
23. Soares, M. B., dos Santos, E. F., Sinisterra, R. D., & Cortés, M. E. (2017). Nanostructured zinc oxide particles for glucose uptake enhancement in Saccharomyces cerevisiae. Biochemical Engineering Journal, 123, 127-134.

24. Zhang, X., Chen, X., Liu, Z., Wu, W., & Zhang, J. (2018). Effect of Ruthenium Doping on the Optical Properties of ZnO Nanoparticles. Journal of Nanoscience and Nanotechnology, 18(4), 3005-3009.
25. Ahmad, M., Ahmed, E., Ahmed, Z., Arshad, M., Awan, M. S., Khan, Z. R., ... & Mahmood, K. (2020). Optical and structural analysis of ruthenium-doped ZnO nanoparticles synthesized by a green route. Materials Research Express, 7(11), 115003.
26. Wang, Z., Hu, S., Ma, J., Chen, C., Zhao, S., Wang, J., & Liu, X. (2019). Influence of ruthenium doping on the structural, electrical and optical properties of ZnO thin films prepared by RF magnetron sputtering. Applied Surface Science, 487, 1232-1238.
27. Tanwar, A., Singh, R., & Kaur, I. (2019). Effect of ruthenium doping on structural and optical properties of ZnO nanoparticles. Journal of Materials Science: Materials in Electronics, 30(19), 17634-17641.
28. Santhoshkumar, T., & Rajenderan, V. (2019). Synthesis, characterization, and catalytic applications of Ru-doped ZnO nanoparticles. Materials Today: Proceedings, 18, 1482-1488
29. Akram, M. A., & Sabir, S. (2018). Synthesis, characterization, and antimicrobial activity of ruthenium-doped zinc oxide nanoparticles. Journal of Nanostructures, 8(3), 245-252.
30. Rani, M., & Shanker, U. (2020). Green synthesis of TiO2 and its photocatalytic activity. In Handbook of Smart Photocatalytic Materials (pp. 11-61). Elsevier.
31. Ismael, M. (2019). Highly effective ruthenium-doped TiO 2 nanoparticles photocatalyst for visible-light-driven photocatalytic hydrogen production. *New Journal of Chemistry*, *43*(24), 9596-9605.
32. Raghupathi, K. R., Koodali, R. T., & Manna, A. C. (2011). Size-dependent bacterial growth inhibition and mechanism of antibacterial activity of zinc oxide nanoparticles. Langmuir, 27(7), 4020-4028.